Invited Paper

Nano-optical studies of superconducting nanowire single-photon detectors

Robert H. Hadfield[a] Paul A. Dalgarno [a], John A. O'Connor [a], Euan J. Ramsay [a], Richard J. Warburton [a], Eric J. Gansen[b], Burm Baek[c], Martin J. Stevens[c], Richard P. Mirin[c], Sae Woo Nam[c]
[a]School of Engineering and Physical Sciences, Heriot-Watt University, Edinburgh, EH14 4AS, United Kingdom;
[b]Department of Physics, University of Wisconsin-La Crosse, 1725 State Street, La Crosse, WI 54601, USA
[c]National Insitute of Standards and Technology, 325 Broadway, Boulder, CO 80305, USA

ABSTRACT

We report on the photoresponse mapping of nanowire superconducting single-photon detectors using a focal spot significantly smaller than the device area (10 μm x 10 μm). Using a solid immersion lens we achieve a spot size of 320 nm full-width half maximum onto the device at 470 nm wavelength. We compare the response maps of two devices: the higher detection efficiency device gives a uniform response whereas the lower detection efficiency device is limited by a single defect or constriction. A second optical setup is used to simultaneously image and measure the photoresponse of the lower detection efficiency device, allowing the constriction location to be pinpointed.

Keywords: Single-photon detector, superconducting detector, nano-optics, solid immersion lens

1. INTRODUCTION

Recent advances in optics and nanotechnology allow light-matter interactions to be probed on ever-diminishing length scales, and hold the key to insights into fundamental physics and the development of new technologies. In this article we apply the techniques of nano-optics (namely confocal microscopy [1] in conjunction with a high refractive index solid immersion lens (SIL) [2-5]) to focus light with sub-micron precision onto nanostructured superconducting wires, and to map their photoresponse.

Superconducting single-photon detectors (SSPDs) based on superconducting nanowires hold promise as a new type of high-speed, high sensitivity single-photon detector, with a spectral range from the visible well into the infrared. The basic device concept was pioneered by Gol'tsman [6]: a 100 nm wide wire is patterned by electron beam lithography and etching in an ultrathin (4 nm thick) NbN superconducting film. The superconducting wire (operated in the temperature range 1.5 – 4 K) is biased close to its critical current, I_C: the arrival of a visible or infrared photon perturbs the current distribution, triggering a fast voltage pulse with picosecond rise time. The current generation of SSPD [7] consists of a meander wire (100 nm linewidth, 200 nm period) covering a 10 μm x 10 μm area, compatible with a single mode telecommunications fiber [8]. These detectors have been successfully employed in a range of applications at the frontiers of science and technology, spanning quantum cryptography [9,10], quantum emitter characterization [11 - 15], time-of-flight ranging [16], testing of integrated circuits [17] and high-speed communications [18]. Recent studies have highlighted the challenges in creating large area nanowire devices [19,20]: defects or constrictions arising from the basic film or during processing are believed to limit the yield. To date the presence of constrictions has been inferred indirectly from critical current [19, 20] and inductance [20] measurements. Optical characterization can offer a direct measurement, but has typically only been carried out using a spot significantly larger than the device area [7, 21]. In this study [22] we map the photoresponse of nanowire SSPDs with unprecedented resolution. We study two devices, and show that the higher detection efficiency (DE) device has a uniform photoresponse, whereas the lower DE device is photosensitive at a single spot. Furthermore, using a second scanning setup we are able to pinpoint the constriction position in the latter device. This study also serves to signpost new strategies for achieving efficient optical coupling to nanostructured detectors.

Quantum Communications Realized II, edited by Yasuhiko Arakawa, Masahide Sasaki, Hideyuki Sotobayashi,
Proc. of SPIE Vol. 7236, 72360G · © 2009 SPIE · CCC code: 0277-786X/09/$18 · doi: 10.1117/12.819360

2. EXPERIMENTAL METHODS

2.1 Set up 1: High resolution photo response mapping

The first mapping setup is shown in figure 1a. This configuration allows excellent optical and spatial resolution, combining a confocal microscope (composed of aspheric lenses) with XYZ piezoelectric translation stages at 4.2 K. The camera assists optical alignment. The sample space is filled with He vapor and the microscope is immersed in liquid He. The resolution limit by Sparrow's criterion [23] is

$$FWHM = \frac{0.52\lambda}{n.NA} \quad (1)$$

where *FWHM* is the full width at half maximum of the focal spot, λ is the wavelength, *NA* is the numerical aperture of the objective lens and *n* is the refractive index. This formula assumes plane wave illumination, but gives a fair approximation for a truncated Gaussian beam. A high refractive index hemispherical SIL allows an enhancement in resolution (compared to free space) by a factor of *n.* This setup is routinely used in the spectroscopy of individual semiconductor quantum dots [3, 5, 24, 25]. We use a LaSFN35 glass SIL with n = 2.0. XYZ piezo motors allow movement in sub-100 nm steps over a range of several mm, but with imperfect stitching characteristics. An additional XY piezo scanner stage allows precision scanning over a 12 μm x 12 μm area. An indium tin oxide filter placed in the optical path to reduce 300 K black body radiation. The minimum temperature attained by the sample stage is 4.9 K. Photodetection events are read out from the SSPD via a bias tee and high-speed room temperature amplifiers, feeding pulses into a counter.

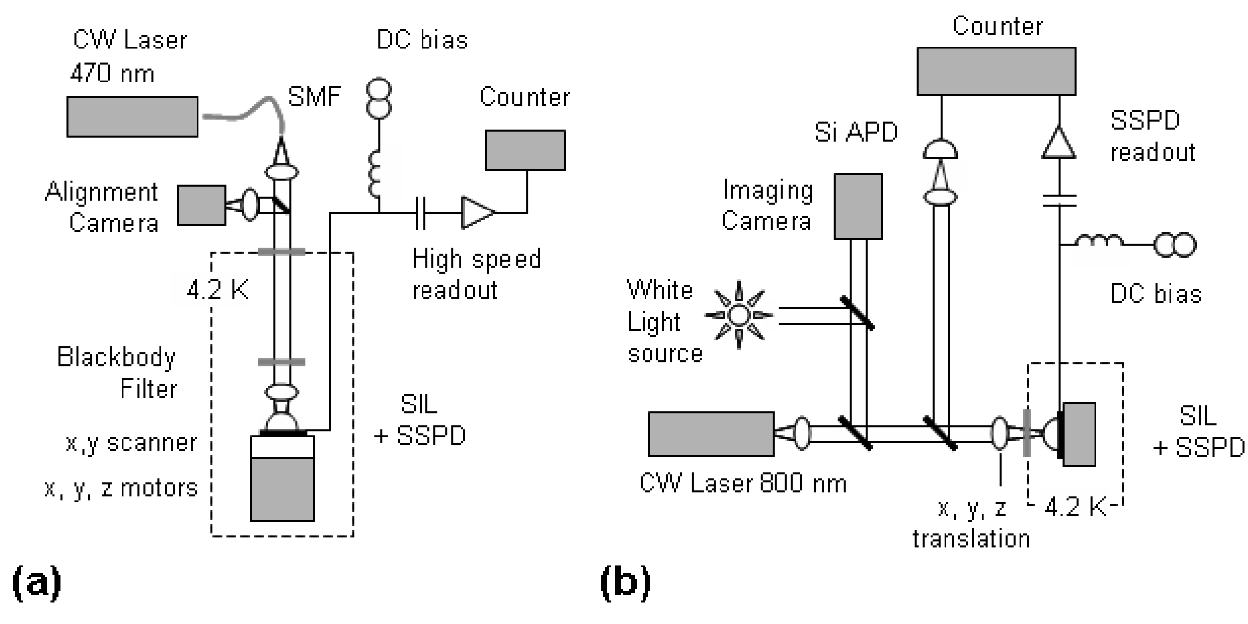

Figure 1: Photoresponse mapping setups. In both cases the device is electrically connected, for biasing and readout of photodetection events. SSPD – nanowire superconducting single photon detector; SIL – hemispherical solid immersion lens; Si APD – silicon avalanche photodiode; SMF – single mode optical fibre; CW laser – continuous wave laser.
Figure 1a: Configuration for high resolution scanning over a small area (12 μm x 12 μm without SIL, 6 μm x 6 μm with n=2.0 SIL). The confocal microscope has a short working distance and high *NA*. The sample is mounted on a low temperature piezoelectric translation stage.
Figure 1b: Configuration for lower resolution, large area mapping. This setup has a longer working distance and hence lower *NA*. This setup allows more versatility, as the full device can be imaged using white light illumination and also reflected signal can be recorded using a Si APD, whilst the APD is read out.

2.2 Set up 2: photo response mapping and imaging

The second mapping setup is shown in figure 1b. This configuration has a longer working distance and poorer resolution, but affords more versatility than the first configuration and thus yields valuable complementary data. This setup allows a wide area to be illuminated and imaged using a white light source and camera. Furthermore, whilst the laser spot is rastered across the device, the reflected signal from the surface of the device is recorded using a silicon avalanche photodiode (Si APD), in addition to the direct SSPD readout. This provides a reference for the photoresponse data relative to reflective features (such as Au contact pads) on the sample surface. The room temperature scanning optics permit translation of the focal spot over a 30 μm x 60 μm area. The sample is in vacuum and heat sunk to a liquid He bath. The working distance is 5 cm and the maximum *NA* is 0.1. Optical access is via BK7 glass windows at 300 K and 4.2 K. At $\lambda = 800$ nm the FWHM spot size from (1) is 4.2 μm without a SIL and 2.1 μm with an n=2.0 SIL.

3. RESULTS

For this study we selected two nanowire SSPD of equal dimensions (100 nm linewidth, 200 nm pitch, 10 μm x 10 μm area), but differing DE and electrical properties. Using our standard fiber coupling technique in a closed-cycle adiabatic demagnetization refrigerator, at $\lambda = 1550$ nm the first device had a DE of 0.3 % at 4.0 K and 0.5 % at 1 K and an ungated dark count rate of 1 kHz. The inductance of this device measured at 4.0 K showed an upturn of 8 % towards I_C of 22 μA (figure 2a inset (ii)), indicating a large proportion of the wire is biased close to the critical current density (J_C) [19]. The absolute inductance value is strongly dependent on film thickness and composition, and gives little indication of device quality. In contrast, the DE of the second device when fiber-coupled was 10^{-6} at $\lambda = 1550$ nm (1 kHz dark count) and 4.0 K. I_C at 4.0 K was just 3 μA. The inductance of this device changes by less than 2 % towards the I_C (Figure 2b, inset (ii)) indicating that most of the wire is biased well below J_C, owing to a defect or constriction in the nanowire [19].

We mounted the higher DE SSPD in the confocal microscope (figure 1a). Using an objective with a *NA* of 0.4 (but no SIL) we mapped the entire device using a continuous wave (CW) laser at $\lambda = 470$ nm and a pulsed diode laser at $\lambda = 410$ nm at 4.9 K. A qualitatively identical response was seen in both cases, over a range of bias points and photon fluxes. Figure 2a shows a uniform plateau over the full 10 μm x 10 μm device area, with counts per second acquired at each point. The background count rate for this scan was ~100 Hz. The photon flux was 10^8 photons per second. The photoresponse varies across the device by just a factor of two, with broad peaks in two regions of the device separated by a slight diagonal trough. The spot resolution is determined from fitting the profile at the device edge. The differentiated fit yields a spot profile (640 nm *FWHM*) close to the resolution expected from (1) (610 nm *FWHM*). DE for the focused spot positioned on the most sensitive area of the device was 0.2 % at 1 kHz ungated dark count rate. This is a fair correspondence to the fiber-coupled measurements on this device, although one would expect improved DE due to the shorter wavelength [10] and the improved optical coupling. In these scanning measurements the thermal environment and blackbody load on the device differs from the fiber-coupled experiments, resulting in an elevated operating temperature (4.9 K) and a reduction in DE at a given dark count rate.

We then mapped the lower DE SSPD at $\lambda = 470$ nm in the setup of figure 1a. We employed a hemispherical SIL (n=2.0) and lens with *NA* 0.36 to enhance the optical resolution (the increased magnification reduces the scan range by a factor of n, to 6 μm x 6 μm). The full device area was mapped in a sequence of scans. The device responds at just a single point. Figure 2b shows a photoresponse map centered on the single photosensitive spot over a 2.16 μm x 2.16 μm area. A qualitatively identical response was seen over a range of bias points and photon fluxes. The *FWHM* of the peak (from a Gaussian fit) in orthogonal directions is 313 nm and 440 nm (inset (ii)), which is close to the theoretical resolution limit (Equation (1) yields a *FWHM* of 340 nm). The Airy disk profile is exaggerated by spherical aberrations and the SIL; the slight asymmetry in the lower profile can be attributed to tilt in the optical path. We can therefore confirm that the sensitive spot is significantly smaller than the optical resolution. Using these enhanced optics the maximum DE was 10^{-5} (at 1 kHz dark count rate) again indicating that the sensitive area is much smaller than our spot size.

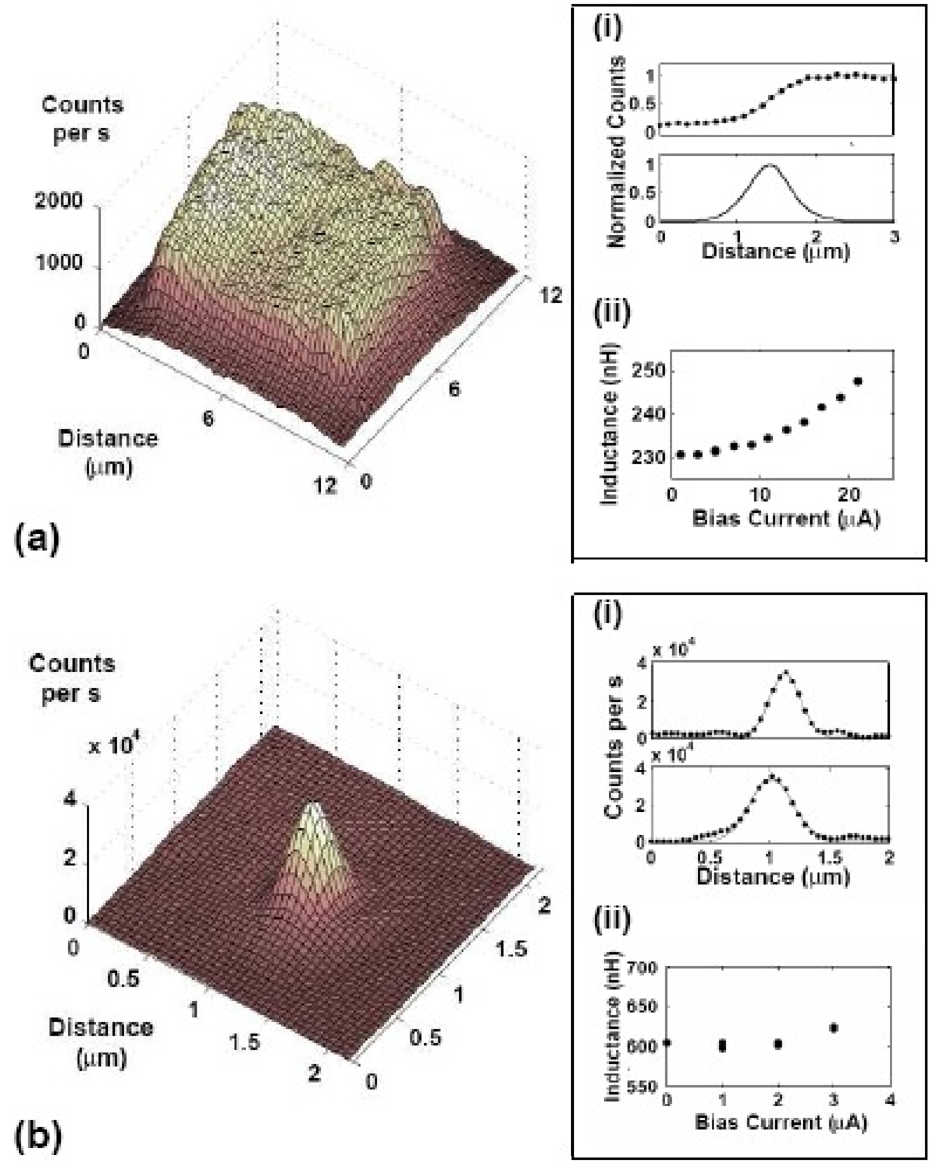

Figure 2 Photoresponse signatures of nanowire SSPDs (using setup depicted in figure 1a). Sample temperature 4.9 K.

Figure 2a: Higher detection efficiency (DE) 10 μm x 10 μm area device. No SIL, NA=0.4, λ = 470 nm, scanning area 12 μm x 12 μm. Inset (i), upper trace: profile of high resolution scan over edge with fit. In the lower trace the FWHM from the differentiated fit is 620 nm. Inset (ii) inductance versus bias current at 4.0 K. The inductance at zero bias is 230 nH and increases by 8 % towards the critical current (22 μA).

Figure 2b: Lower DE10 μm x 10 μm area device. SIL *n*=2.0, *NA*=0.36, λ = 470 nm, high resolution scan of 2.16 μm x 2.16 μm area. Inset (i) profiles in orthogonal scanning directions: FWHM from Gaussian fits, 313 nm and 430 nm respectively. Inset (ii) inductance versus bias current at 4.0 K. The inductance at zero bias is 600 nH and increases by 3 % towards the critical current (3 μA).

In order to determine the position of the defect in the lower DE device we employ the second configuration (figure 1b). Figure 3a shows a scanning electron micrograph (SEM) of the device. At λ=800 nm using an objective of NA = 0.1 and an n=2.0 SIL, we obtain a spot size of ~ 2.1 μm (reducing the scan area to 15 μm x 30 μm). The device photoresponse is shown in Figure 3b – as expected just a single point (broadened by the beam profile) is photosensitive. The reflected signal from the Au bowtie (measured in tandem) gives a clear signature as shown in Figure 3c. The constriction is located at the edge of the meander, where the wire switches back on itself – and is marked 'x' in Figures 3a and 3c.

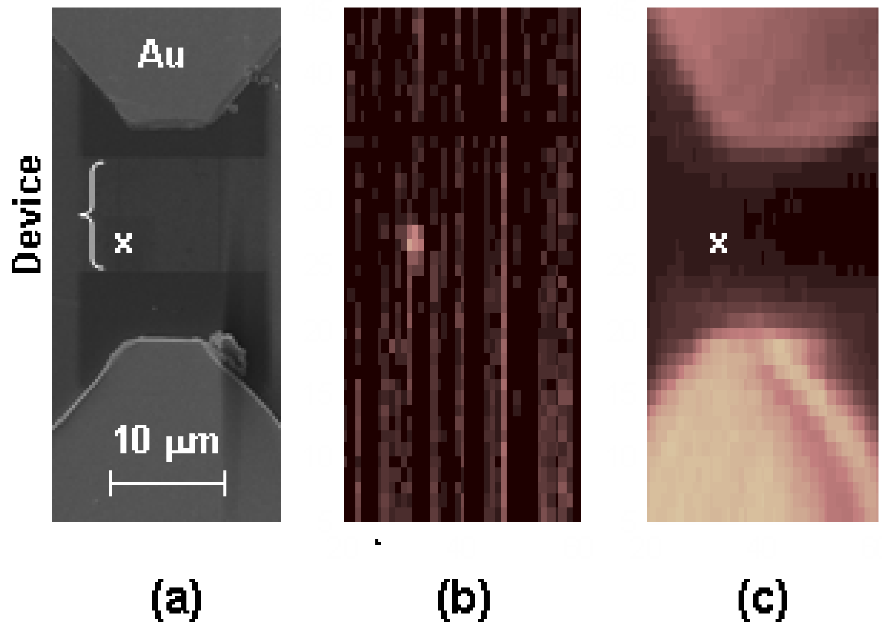

Figure 3 Determining the position of the constriction in lower DE SSPD (using setup depicted in figure 1b). The lightest regions in 3b and 3c correspond to maximum count rates on the SSPD and Si APD respectively. The position of the constriction (determined from 3b) is marked 'x' in 3a and 3c. Figure 3a scanning electron micrograph (SEM) of meander (Au labeled). Figure 3b photoresponse map of lower DE SSPD at λ = 800 nm (identical area to 3b) Figure 3c reflection data (measured with Si APD simultaneously with the data in 3b)

4. DISCUSSION

In conclusion, we have successfully mapped the photoresponse of nanowire SSPDs with a focal spot significantly smaller than the device area. We have mapped two SSPDs of contrasting performance: the higher DE device gives a uniform response across the device area, whereas the lower DE device responds at a single point where the nanowire is constricted. Using our second imaging setup we show that the constriction is located at the edge of the meander. We intend to implement a similar scanning setup to image these devices at longer wavelengths (beyond 1 μm). A hyper hemispherical Si super SIL (n=3.5) with an NA =0.4 lens would confer a spot size at λ = 1550 nm of 160 nm [24] and ~110 nm at λ = 1064 nm, allowing us to probe the photoresponse signature of single wires. Photoresponse mapping experiments on conventional Si APD single-photon detectors have yielded significant insights into the spatial dependence of device sensitivity and timing response [25]; we are now in a position to undertake similar studies on superconducting nanowire detectors, over much finer length scales. Furthermore, this enhanced optical coupling technology will allow us to explore novel device designs (e.g. nano-antennas), which may prove easier than the current meander design to fabricate with high yield and scale up into multi-pixel arrays.

Acknowledgements:
This work was supported by the Royal Society and EPRSC (United Kingdom) and DARPA, DTO and the NIST Quantum Information Science Initiative (USA). The authors thank Gregory Gol'tsman for providing the original devices used in this study and Aaron Miller and Alan Migdall for useful discussions.

REFERENCES

[1] R. H. Webb Rep.Prog. Phys **59** (3) 427-471 (1996)
[2] S. M. Mansfield and G. S. Kino, Appl. Phys. Lett. **57**, 2615 (1990)
[3] V. Zwiller, G. Bjork, J. Applied Physics **92** (2) 660 (2002)
[4] W. L. Barnes, G. Bjork, J. M. Gerard, P. Jonsson, J. A. E. Wasey, P. T. Worthing, V. Zwiller Eur. Phys. J. D **18** 197 (2002)
[5] For a forthcoming review of Solid Immersion Lens applications see K. A. Serrells *et al* submitted to J. Nanophotonics
[6] G. N. Gol'tsman, O. Okunev, G. Chulkova, A. Lipatov, A. Semenov, K. Smirnov, B. Voronov, A. Dzardanov, C. Williams, R. Sobolewski, Appl. Phys. Lett. **79** (6) 705 (2001)
[7] Verevkin, J. Zhang, R. Sobolewski, A. Lipatov, O. Okunev, G. Chulkova, A. Korneev, K. Smirov, G. N. Gol'tsman, A. Semenov, Appl. Phys. Lett. **80,** (25) 4687 (2002)
[8] www.corning.com; SMF-28e optical fiber.
[9] R. H. Hadfield, J. L. Habif, J. Schlafer, R. E. Schwall, S. Nam Appl. Phys. Lett. **89** 241129 (2006)
[10] H. Takesue, S. Nam, Q. Zhang, R. H. Hadfield, T. Honjo, K. Tamaki, Y. Yamamoto, **1** (6) 343 Nature Photonics (2007)
[11] R. H. Hadfield, M. J. Stevens, S. S. Gruber, A. J. Miller, R. E. Schwall, R. P. Mirin, S. W. Nam, Optics Express **13,** (26) 10846 (2005)
[12] M. J. Stevens, R. H. Hadfield, R. E. Schwall, S.W. Nam, R. P. Mirin, J. A. Gupta, Appl. Phys. Lett. **89** 031109 (2006).
[13] C. Liang, K. F. Lee, M. Medic, P. Kumar, R. H. Hadfield, P. Kumar Optics Express **15** (3) 1322 (2007)
[14] R. H. Hadfield, M. J. Steven, S. Nam, R. P. Mirin, J. Appl. Phys. **101** 103104 (2007)
[15] C. Zinoni, B. Alloing, L. H. Li, F. Marsili, A. Fiore, L. Lungi, A. Gerardino, Yu B. Vakhtominm, K. V. Smirnov, G. N. Gol'tsman*,* Applied Physics Letters **91** 031106 (2007)
[16] R. E. Warburton, A. McCarthy, A. Walker, S. Hernandez-Marin, R. H. Hadfield, S. Nam, G. S. Buller Optics Letters **32** (15) 2266 (2007)
[17] J. Zhang, N. Boiadjieva, G. Chulkova, H. Deslandes, G. N. Gol'tsman, A. Korneev, P. Kouminov, A. Leibowitz, W. Lo, R. Malinsky, O. Okunev, A. Pearlman, W. Slyz, K. Smirnov, C. Tsao, A. Verevkin, B. Voronov, K. Wilsher, R. Sobolewski, Electronics Letters **39** (14) 1086 (2003)
[18] B. S. Robinson, A. J. Kerman, E. A. Dauler, R. O. Barron, D. O. Caplan, M. L. Stevens, J. J. Carney, S. A. Hamilton, J. K. W. Yang, K. K. Berggren Optics Letters **31** (4) 444 (2006)
[19] F. Mattioli, R. Leoni, A. Gaggero, M. G. Castellano, P. Carelli, F. Marsili, A. Fiore J. Appl. Phys. **101** (5) 054302 (2007)
[20] J. Kerman, E. A. Dauler, J. K. W. Yang, K. M. Rosfjord, V. Anant, K. K. Berggren, G. N. Gol'tsman, B. M. Voronov, Appl. Phys. Lett. **90**, 101110 (2007)
[21] K. M. Rosfjord, J. K. W. Yang, E. A. Dauler, A. J. Kerman, V. Anant, B. M. Voronov, G. N. Gol'tsman, K. K. Berggren, Optics Express **14** (2) 527 (2006)
[22] R. H. Hadfield, P. A. Dalgarno, J. A. O'Connor, E. Ramsay, R. J. Warburton, E. J. Gansen, B. Baek, M. J. Stevens, R. P. Mirin, S. Nam, Appl. Phys. Lett. **91** 241108 (2007)
[23] C. M. Sparrow, Astrophysical Journal **44** 76 (1916).
[24] S. Moehl, H. Zhao, B. D. Don, S. Wachter, H. Kalt, J. Appl. Phys. **93** (10) 6265 (2003)
[25] P. A. Dalgarno, J. McFarlane, B. B. Geradot, R. J. Warburton, K. Karrai, A. Badolato, P. M. Petroff, Applied Physics Letters **89** (4) 043107 (2006)
[26] E. Ramsay, K. A. Serrels, M. J. Thomson, A. J. Waddie, M. R. Taghizadeh, R. J. Warburton, D. T. Reid, Appl. Phys. Lett. **90** 131101 (2007)
[27] M. Ware, A. Migdall, J. C. Bienfang, S. V. Polyakov J. Modern Optics **54** (2-3) 361-372 (2007)